

## **STATUS REPORT 4**

PROJECT TITLE: LOCAL AND GLOBAL ACOUSTIC CONTROL FOR LAUNCH  
VEHICLE PAYLOAD FAIRINGS

INVESTIGATORS: DR. DONALD J. LEO  
MR. KEVIN FARINHOLT

CIMSS / MECHANICAL ENGINEERING DEPARTMENT  
310 NEW ENGINEERING BLDG.  
VIRGINIA TECH  
BLACKSBURG, VA, 24061-0261

TEL: (540) 231-2917  
FAX: (540) 231-2903  
EMAIL: [donleo@vt.edu](mailto:donleo@vt.edu)

PURCHASE ORDER: 00-04-6838

START DATE: 10-MAY-00  
END DATE: 09-MAY-01

### **ACCOMPLISHMENTS SINCE PREVIOUS PROGRESS REPORT:**

Developed a control model of a tapered waveguide for the purpose of understanding the controllability.

### **DISCUSSION**

This report presents work done to model both full-state feedback control as well as observer-based control for the purpose of attenuating acoustic levels within a truncated cone. Through the analysis presented in the following sections, we have found that suitable compensators can be designed using both methods, yielding performance levels which satisfy all of the control specifications set forth in the fourth section of this report. Frequency response and robustness analyses have also been performed on the system to insure stability and insensitivity to model error, each of which are discussed in their respective sections.

#### **Background and Motivation**

Figure 1 illustrates the general geometry used in fairing construction, and it can be seen from this figure that the enclosure possesses geometric discontinuities at either end of the short cylindrical

section. These geometric variations translate into acoustic discontinuities within the enclosure, the result of wave reflections along the fairing walls. The complex nature of these reflection functions compounds the difficulty associated with modeling the acoustic modes in closed form.

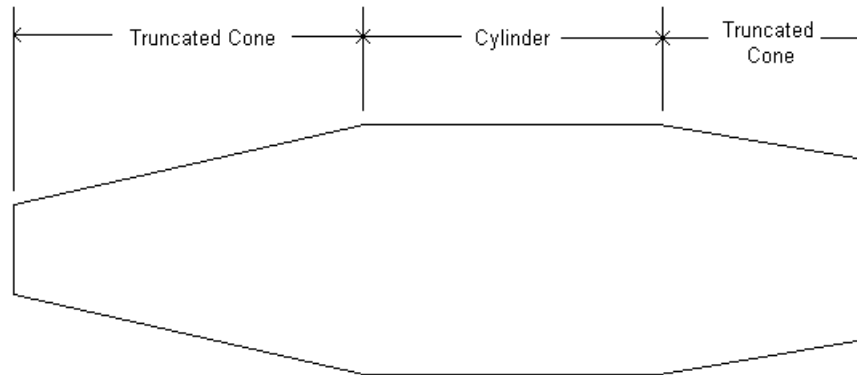


Figure 1. Representative geometry of typical payload fairings.

One possible method for approaching wave propagation within such an enclosure is the generation of a piecewise model. Equating pressure and velocity at boundary conditions would be used to enforce some level of continuity between the sections. For my work in this project for ME 5505, I chose to analyze the first of the three sections that comprise the fairing cavity. If this model were to be used within my actual research, I would have to solve each of the three sections simultaneously, insuring that the boundary conditions are met. However, for the purposes of this project, I chose to consider the case of a truncated cone having rigid end conditions at both the major and minor ends of the enclosure, as shown in Figure 2. For the purposes of studying controllability, I assumed that an external disturbance was acting within the enclosure, with an input located at the minor end of the system to facilitate actuation of the controller.

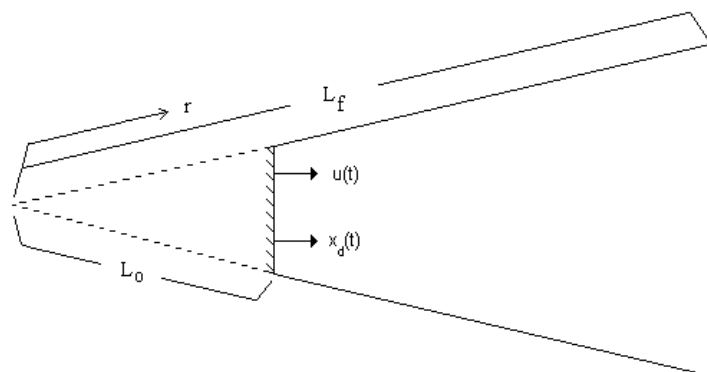


Figure 2. Truncated cone to be studied. ( $L_f = 1.75$  m,  $L_0 = 0.75$  m)

## State-Space Modeling

To properly model the dynamics of this system, it is necessary to consider the generalized wave equation, which is of the form:

$$\Delta^2 P(r,t) = \frac{1}{c^2} \frac{\partial^2 P(r,t)}{\partial t^2} = \frac{\rho_o}{\gamma P_o} \frac{\partial^2 P(r,t)}{\partial t^2} \quad (1)$$

where  $P(r,t)$  = Pressure as a function of location and time  
 $c$  = Speed of sound  
 $\gamma$  = ratio of specific heats, 1.40  
 $P_o$  = ambient pressure within the enclosure, 101.3 E 3 Pascals  
 $\rho_o$  = density of air, 1.206 kg/m<sup>3</sup>  
 $\Delta$  = Laplacian operator

For cylinders, the extreme conic section with  $L_r = \text{infinite}$ , the Laplacian simply becomes the partial derivative with respect to the spatial coordinate. This leads to the common wave equation used in plane wave analysis. Unfortunately, in the case of a conical bore, plane waves are not very applicable due to variations in the bore's cross sectional area. Therefore, it is more appropriate to use spherical wave propagation as a means of modeling the acoustic behavior within a conical bore. One added complication associated with the use of spherical waves is a slightly more involved Laplacian operator. This new Laplacian now contains terms associated with the spatial component, resulting in the following wave equation:

$$\gamma P_o \left[ \frac{1}{r^2} \frac{\partial}{\partial r} \left( r^2 \frac{\partial P(r,t)}{\partial r} \right) \right] = \rho_o \frac{\partial^2 P(r,t)}{\partial t^2} \quad (2)$$

where  $r$  = spatial coordinate

Upon initial inspection, this wave equation takes a form similar to that of the longitudinal vibration in a tapered rod.

$$\frac{\partial}{\partial x} \left( EA(x) \frac{\partial \omega(x,t)}{\partial x} \right) = \rho A(x) \frac{\partial^2 \omega(x,t)}{\partial t^2} \quad (3)$$

Comparing terms between the governing equation (Eqn. 2) for spherical wave propagation, with the governing equation (Eqn. 3) for longitudinal vibration in tapered rods, it can be seen that each side of the equation is roughly equivalent to the corresponding term in the other equation. Equations 4 and 5 illustrate this comparison:

$$\frac{\partial}{\partial x} \left( EA(x) \frac{\partial \omega(x,t)}{\partial x} \right) \approx \gamma P_o \frac{\partial}{\partial r} \left( r^2 \frac{\partial P(r,t)}{\partial r} \right) \quad (4)$$

$$\rho A(x) \frac{\partial^2 \omega(x,t)}{\partial t^2} \approx \rho_o r^2 \frac{\partial^2 P(r,t)}{\partial t^2} \quad (5)$$

By equating the "potential" (Eqn 4) and "kinetic" (Eqn. 5) terms of each equation, it is possible to view the previously ambiguous components of the wave equation in a way that is comparable to that of vibration within a solid rod. Following the same method for solving the tapered bar problem, the function of pressure is reduced to two components through separation of variables, a spatial and a temporal term.

$$P(r,t) = \phi(r)\eta(t) \quad (6)$$

From this point, a Ritz-Galerkin approximation method is used to obtain a series representation of the spatial solution to the wave equation. The system is assumed to have no modal damping present, so that the equation of motion takes the following form:

$$M\ddot{\eta}(t) + K\eta(t) = U \quad (7)$$

where M and K are equivalent mass and stiffness matrices and U is a matrix of inputs. (It must be noted that these are not actually mass and stiffness matrices, they simply take a similar form to those obtained through the analysis of a rod in longitudinal vibration.)

Considering the boundary conditions of the closed-closed conical bore, the spatial derivative of pressure must be zero at both locations. For proper convergence of this approximation method, the admissibility function,  $\phi_i(x)$ , must be chosen such that these boundary conditions are satisfied. This is accomplished through the following function:

$$\phi_i(r) = \frac{-(L_f - L_o)}{i\pi} \cos \left( \frac{i\pi(r - L_o)}{L_f - L_o} \right) \quad (8)$$

$i = 1, 2, \dots, n$

Following the derivation of Meirovitch [1997], equivalent stiffness and mass terms were developed in accordance with the following equations:

$$k_{ii} = \int_{L_o}^{L_f} \phi_i(r) \frac{\partial}{\partial r} \left[ \gamma P_o r^2 \frac{\partial \phi_i(r)}{\partial r} \right] dr \quad (9)$$

$$k_{ij} = \int_{L_o}^{L_f} \phi_i(r) \frac{\partial}{\partial r} \left[ \gamma P_o r^2 \frac{\partial \phi_j(r)}{\partial r} \right] dr \quad (10)$$

$$m_{ii} = \int_{L_o}^{L_f} \phi_i(r) \rho_o r^2 \phi_i(r) dr \quad (11)$$

$$m_{ij} = \int_{L_o}^{L_f} \phi_i(r) \rho_o r^2 \phi_j(r) dr \quad (12)$$

The Mathematica code included as appendix A was used to evaluate each of these integrals over the range of integration. Applying the corresponding indices,  $i=1,2,3$  and  $j=1,2,3$ , generalized mass and stiffness matrices were obtained, each of which are associated with the first three acoustic modes of the truncated conical bore shown in figure 2. Solving for the eigenvalues and eigenfunctions associated with these equations, the following expression was obtained for the pressure variation within the cavity.

$$P(x,t) = [0.3180 \cos(3.14(r - L_o)) - 0.00602 \cos(6.28(r - L_o)) + 0.000426 \cos(9.42(r - L_o))]h_1(t) \\ + [0.0121 \cos(3.14(r - L_o))] + 0.158943 \cos(6.28(r - L_o)) - 0.00370 \cos(9.42(r - L_o))]h_2(t) \quad (13) \\ + [-0.000858 \cos(3.14(r - L_o)) + 0.00557 \cos(6.28(r - L_o))] + 0.106 \cos(9.42(r - L_o))]h_3(t)$$

Again, it must be said that this equation is composed of only the first three modes of vibration. A more complete solution could be obtained by increasing the number of modes included, accomplished through the generation and analysis of larger mass and stiffness matrices. While the pressure equation is an important component in understanding the behavior of acoustics within the enclosure, for controllability purposes, it is more appropriate to represent the system in the form of Eqn. 7. Rearranging the coefficients of Eqn. 7 as follows, a state space model of the system can be easily obtained.

$$\dot{\eta}(t) = -M^{-1/2}KM^{-1/2}\eta(t) + M^{-1/2}UM^{-1/2} \quad (14)$$

Selecting six states to represent the system, three associated with the temporal component of each mode,  $\eta_1(t)$ ,  $\eta_2(t)$ ,  $\eta_3(t)$ , and three more associated with the time derivative of these first three states.

$$\begin{aligned}
x_1 &= \eta_1(t) & x_3 &= \eta_2(t) & x_5 &= \eta_3(t) \\
x_2 &= \dot{\eta}_1(t) & x_4 &= \dot{\eta}_2(t) & x_6 &= \dot{\eta}_3(t)
\end{aligned} \tag{15}$$

Generating the corresponding state matrices, the state-space representation is composed of the following set of matrices:

$$A = \begin{bmatrix} 0 & 1 & 0 & 0 & 0 & 0 \\ -1.08E6 & 0 & -1.39E5 & 0 & 3.08E4 & 0 \\ 0 & 0 & 0 & 1 & 0 & 0 \\ -1.39E5 & 0 & -4.78E6 & 0 & -2.07E5 & 0 \\ 0 & 0 & 0 & 0 & 0 & 1 \\ 3.08E4 & 0 & -2.07E5 & 0 & -1.07E7 & 0 \end{bmatrix} \quad B = \begin{bmatrix} 0 \\ 21.46 \\ 0 \\ 80.57 \\ 0 \\ 125.3 \end{bmatrix} \tag{16}$$

$$C = [1 \quad 0 \quad 1 \quad 0 \quad 1 \quad 0] \quad D = [0]$$

An interesting characteristic of this system is the extreme range of values associated with the A matrix. Calculating controllability and observability matrices for this system yields components ranging in value from 1 E0 to those on the order of 1 E16. Interestingly, this poses a problem when calculating the rank of the Q and N matrices. MATLAB utilizes 15-point precision in its calculations, such that the value of the smallest terms approaches 0, resulting in a rank less than the number of states in the system. To check the true rank of the system, it is possible to divide the first, third and fifth columns by a constant, reducing their order. If this constant is the same for all three columns, the system is simply scaled, and the rank can be solved for without errors introduced by numeric precision.

### Control Specifications

Given that the purpose of this system is the reduction of acoustic loads acting on satellite components during launch, the two most important design parameters are maximum output and settling time. Maximum output pressure is the most important component of the design, considering that the application of a control effort should not exceed greatly the levels associated with the internal acoustics. If the actuator were to generate signals of greater magnitude than those present due to the disturbance, the benefits of reducing overall acoustic levels would be at the cost of short pressure impulses resulting from the control actuator. To monitor this impact, the output of the temporal component of pressure is calculated at the minor end of the conic section since this will be the location of maximum pressure within the fairing. An actual value for this condition is difficult to ascertain, so for this control study, I designed the pole locations to simply minimize the maximum output of the system.

Another important design parameter is the settling time of the response. Ideally, pressure variations induced by unwanted sources should be driven to zero as quickly as possible. Therefore, as a constraint secondary to the minimization of output, the response to disturbance forces should be minimized as well. Appropriate values for this constraint, obtained from initial iterations appear to be settling times less than 0.02 seconds when considering a step input as the disturbance signal.

### Full-State Feedback Design

Following the development of a suitable state-space representation of the dynamics of the acoustic cavity, along with the establishment of desirable performance characteristics, the design of a full-state feedback compensator was begun. Looking at the open loop pole locations, it can be seen that the system operates with no modal damping present.

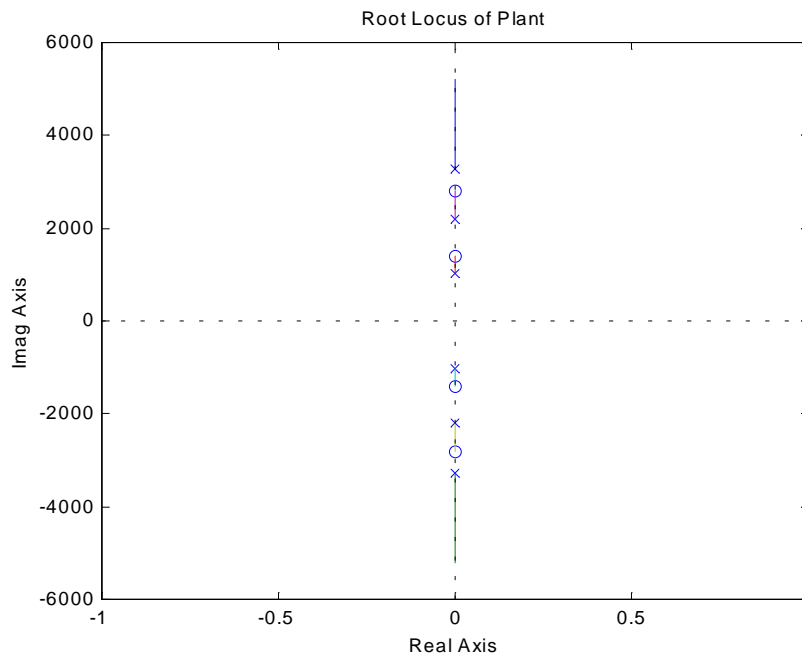


Figure 3. Plot of open-loop pole locations.

Using this root locus for design purposes, only two conclusions can be drawn. The first of these conclusions relates to the speed of the system response. Including a vertical line in the  $s$ -plane will define a region to the left of which will satisfy the settling time constraint. The second conclusion is a qualitative statement concerning the amount of modal damping present. Since this system initially has no damping present, the closed loop poles must be moved into the left half plane; with increased damping the closer the poles are placed to the real axis.

Therefore, to begin the full-state feedback design, small additions to the real component of the pole locations were investigated to force an eventual decay of the response. Table 1 lists several of the iterations conducted to obtain the final compensator design. Row nineteen of this table lists the most attractive pole locations as well as the performance associated with them. Moving the closed loop poles to locations of  $-650 \pm 863i$ ,  $-684 \pm 1509i$ , and  $-440 \pm 2425i$  minimizes the maximum output, while maintaining a relatively low settling time. From the iterations performed in the design process, the most feasible pole locations were obtained by moving the poles further away from the imaginary axis while pulling them in toward the real axis.

Table 1. Summary of Design Iterations

It.	Pole Locations (conjugate pairs)									Max Press. (Pa)	Settling Time	Max FSF Gain			
	Pole 1			Pole 2			Pole 3								
1	10	+/-	646	i	12	+/-	862	i	8	+/-	647	i	150.36	0.100	1.46E+05
2	10	+/-	862	i	12	+/-	1293	i	8	+/-	1293	i	3.83	0.100	1.12E+05
3	100	+/-	862	i	120	+/-	1293	i	80	+/-	1293	i	1.10	0.046	1.10E+05
4	5000	+/-	862	i	6000	+/-	1293	i	4000	+/-	1293	i	0.24	0.003	1.16E+07
5	1000	+/-	862	i	1200	+/-	1293	i	800	+/-	1293	i	0.17	0.008	7.10E+04
6	500	+/-	862	i	720	+/-	1293	i	400	+/-	1293	i	0.52	0.011	5.47E+04
7	500	+/-	862	i	720	+/-	1293	i	400	+/-	1293	i	0.52	0.011	5.47E+04
8	550	+/-	862	i	720	+/-	1293	i	400	+/-	1293	i	0.50	0.011	5.13E+04
9	650	+/-	862	i	600	+/-	1293	i	440	+/-	1293	i	0.47	0.012	4.99E+04
10	650	+/-	862	i	660	+/-	1293	i	440	+/-	1293	i	0.45	0.011	4.55E+04
11	650	+/-	862	i	684	+/-	1293	i	440	+/-	1293	i	0.44	0.011	4.38E+04
12	620	+/-	862	i	684	+/-	1293	i	416	+/-	1293	i	0.47	0.011	4.78E+04
13	650	+/-	970	i	684	+/-	1293	i	440	+/-	1293	i	0.40	0.012	4.21E+04
14	650	+/-	646	i	684	+/-	1293	i	440	+/-	1293	i	0.55	0.010	4.66E+04
15	650	+/-	862	i	684	+/-	1616	i	440	+/-	1293	i	0.30	0.010	3.44E+04
16	650	+/-	862	i	684	+/-	970	i	440	+/-	1293	i	0.66	0.011	5.11E+04
17	650	+/-	862	i	684	+/-	1293	i	440	+/-	2101	i	0.13	0.007	2.10E+04
18	650	+/-	862	i	684	+/-	1616	i	440	+/-	2101	i	0.08	0.009	1.81E+04
19	<b>650</b>	<b>+/-</b>	<b>862</b>	<b>i</b>	<b>684</b>	<b>+/-</b>	<b>1509</b>	<b>i</b>	<b>440</b>	<b>+/-</b>	<b>2425</b>	<b>i</b>	<b>0.07</b>	<b>0.007</b>	<b>1.76E+04</b>
20	650	+/-	862	i	684	+/-	1509	i	440	+/-	2909	i	0.04	0.008	2.35E+04

In designing the controller for this application, reference tracking was considered less important than disturbance rejection, so  $x_r(t)$  was set equal to zero. Gain values,  $G_o$ , were calculated for the system, however all of the gains associated with the reference input were irrelevant since they were each applied to a reference state of zero value. The only gain of importance was therefore the gain associated with the disturbance input,  $x_d(t)$ , which was assumed to be a step input. Simulation of this system can be seen in figure 4a, with a plot of the corresponding control effort in figure 4b.

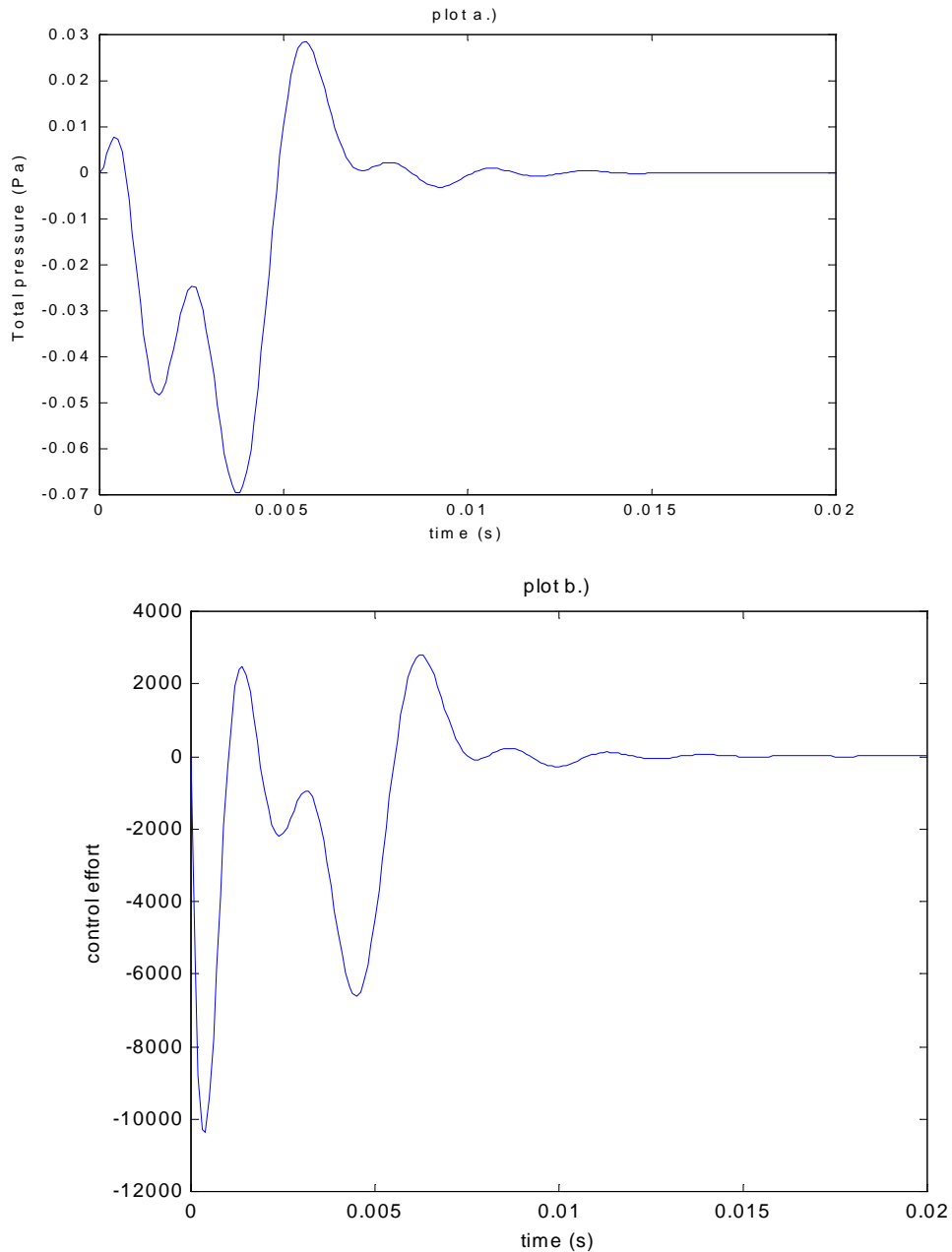


Figure 4.  
 Plot 4a.) Simulation of full-state feedback system to a step disturbance input  
 Plot 4b.) Control effort associated with full-state feedback system

From the first plot in this figure, it can be seen that the maximum output was on the order of 0.0696 Pa, with a settling time of 0.0069 s. Through the iterations performed, it was found that these pole locations serve to keep the maximum output values low, with settling time falling within the acceptable range of 0.02 seconds discussed in the control specifications section of this report. Observation of the control effort associated with this system is also of importance, yielding a maximum value for  $-Gx(t)$  on the order of  $10^4$ , levels which should be acceptable for

this application. From these conclusions, the successfulness of applying full-state feedback techniques to the issue of acoustic control within a truncated conical bore has been proven.

### Observer-based Compensator Design

Following standard techniques for observer-based design, a system observer was developed, operating with pole locations five times faster than those of the full-state feedback system of the previous section. Re-deriving the system equation of the observer-based system to take into account exogenous inputs, the following relationship for the input matrix  $B$  were obtained:

$$B_{\text{obs}} = \begin{bmatrix} BG - BG_r & F - BG_d \\ BG - BG_r & F - BG_d \end{bmatrix} \quad (17)$$

Simulating this new observer-based system with a step disturbance, the following comparison of system responses for full-state feedback and observer-based designs was obtained.

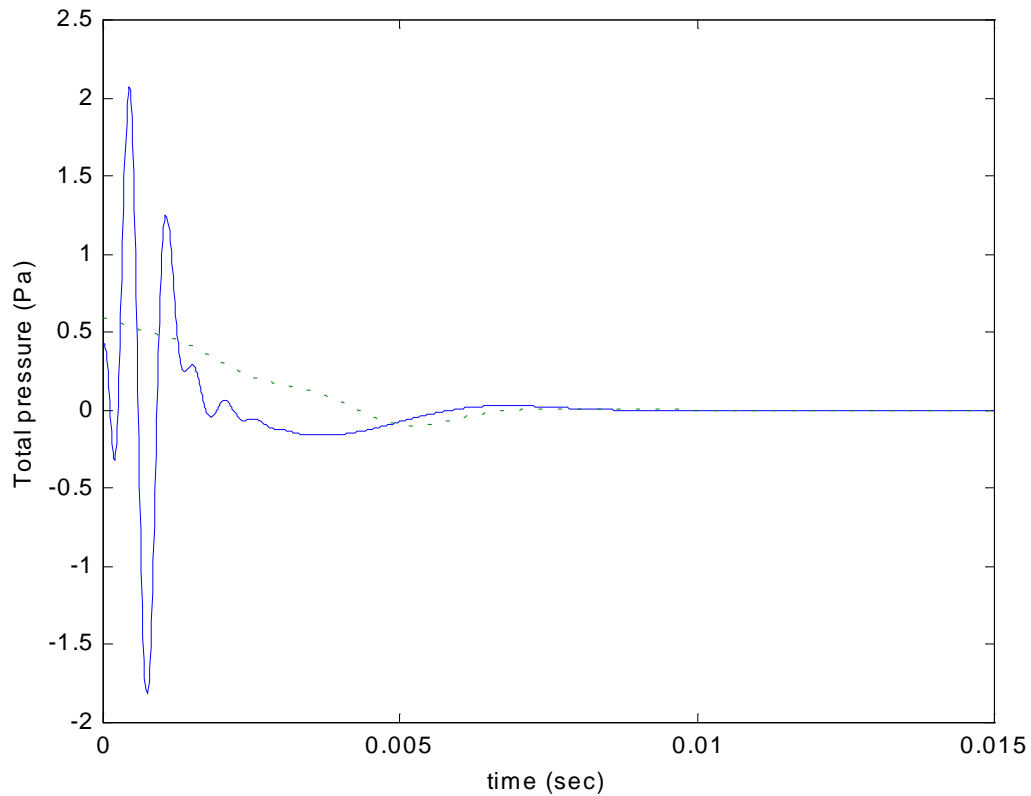


Figure 5. Comparison of response: full-state feedback (dashed), observer-based design (solid)

From this figure, it can be seen that the observer-based system converges to the full-state feedback system within 0.01 seconds, with maximum outputs approximately four times those of the full-state feedback design.

### Frequency response analysis of Controller

Following the design of an observer-based compensator, a frequency response analysis of the compensator was performed. Plotting the bode plot of the open-loop plant and compensator can be seen in figure 6.

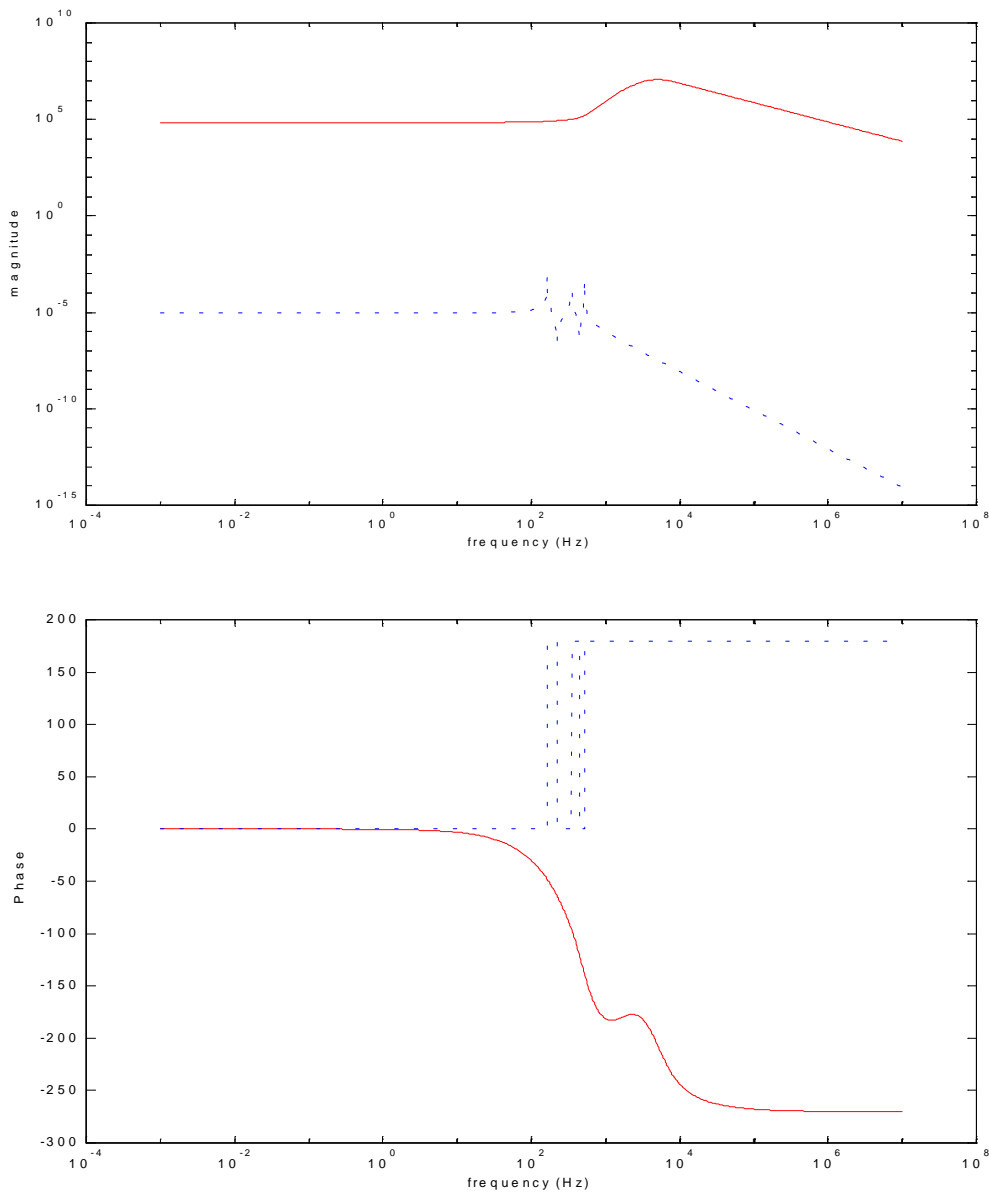


Figure 6. Frequency Response of the plant (dashed) and the compensator (solid)  
Plot 6a. Magnitude. Plot 6b. Phase

Looking at the compensator, the corresponding phase margin is equal to 90 degrees, with and infinite gain margin since the phase never passes through 0 or 360 degrees. The frequency response for the plant illustrates that the system is marginally stable, a conclusion drawn from the fact that both the gain and phase margin are zero at each crossover frequency. Multiplying the compensator by the plant, a model for the entire open-loop system is obtained. Performing a frequency response of this entire system results in the frequency response of figure 7.

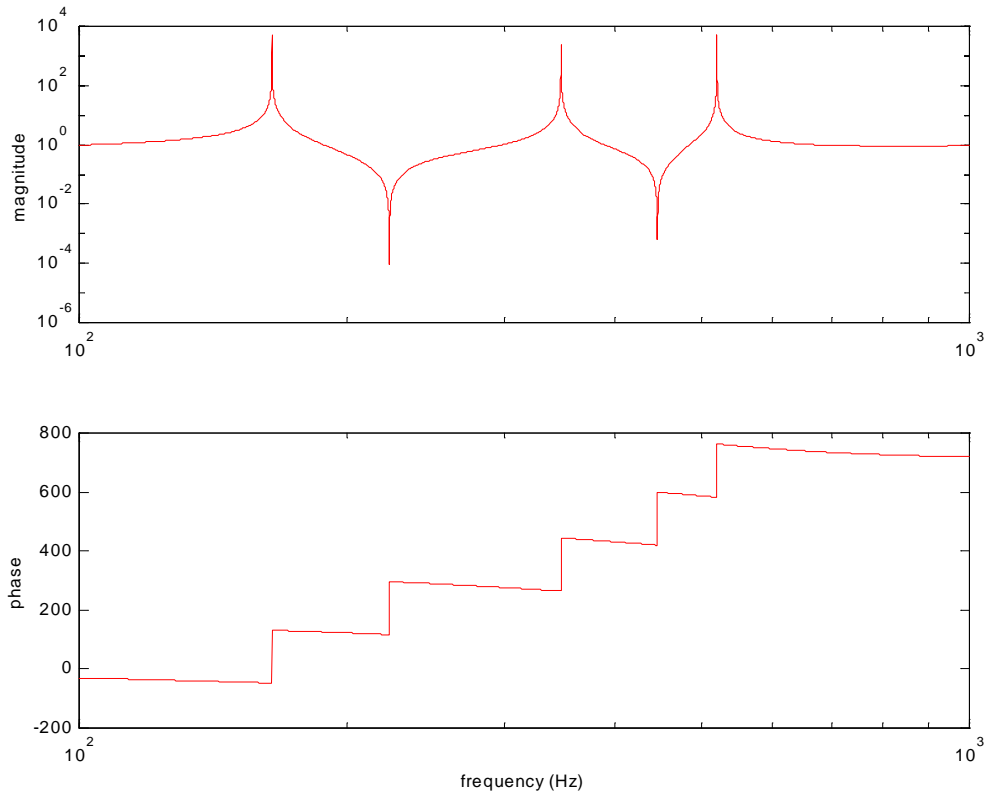


Figure 7.) Frequency response of total open-loop system (compensator\*plant)

Due to the absence of modal damping in the plant, the frequency response of the total system still appears to be marginally stable. Since this system is a SISO system with constant inputs, Nyquist analysis can also be applied to determine stability. Figure 8 is the Nyquist plot for the total open-loop system. Looking at this plot over an extended range of frequencies it can be seen that no encirclements of the -1 point exist, indicating that the total system is in fact stable.

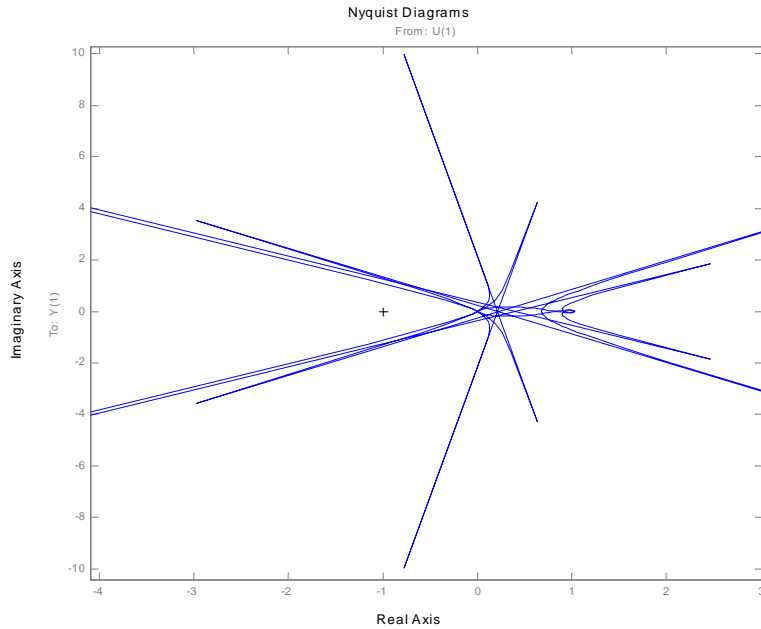


Figure 8.) Nyquist analysis of the total system

Another point of interest in the frequency response analysis of the compensator is the effect of varying the observer gain matrix  $K$ . Varying the observer pole locations  $\pm 40\%$  of the optimal pole locations, transfer functions were obtained with frequency responses plotted in figure 9.

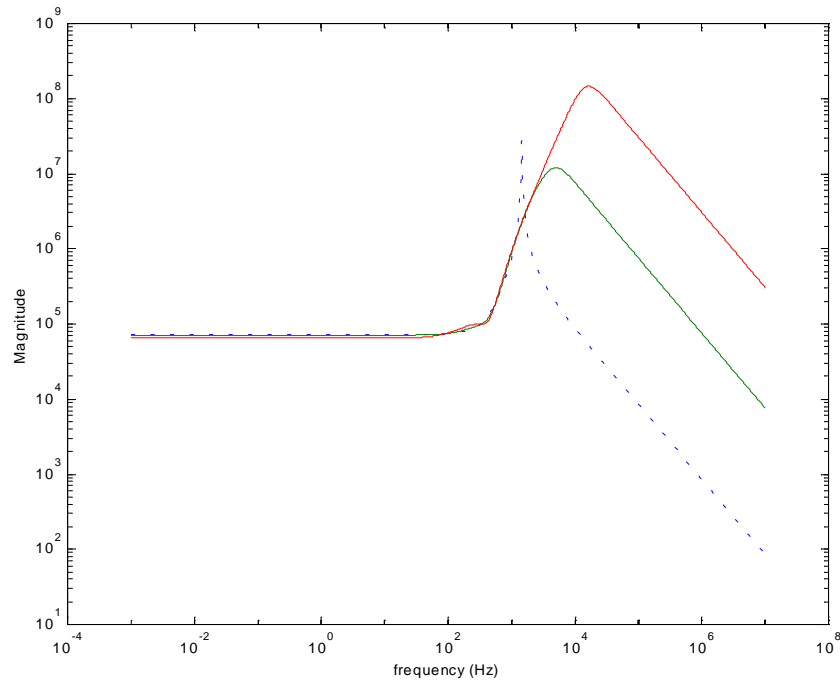


Figure 9.) Frequency response of different observer designs

Simulating each of these compensators to a step disturbance input yields the expected effects on settling time and maximum output. As the poles of the observer slow down, the maximum output decreases, but at the cost of increased settling time. Conversely, as the observer speeds up, the settling time decreases at the cost of increased output levels. Some iterations were performed on observer pole locations and it was found that suitable performance was obtained where the observer poles were approximately 5 times faster than those of the full-state feedback design.

### Robustness Analysis

Looking at the robustness of the closed-loop compensator for 20% variations in each of the three modes, the following plot of settling time versus  $\Delta A$  is obtained. From this plot it can be seen that the robustness is asymmetric relative to the operating point. Overestimation of the plant components, i.e. a softer stiffness matrix, is less detrimental to the system than are underestimations. So long as the plant model is within 5% of the physical system, the controller performance will function well. If, however, the model underestimates the plant by more than 5%, the settling time increases by at least 50%, with another sharp increase in  $t_s$  at  $\Delta = 18\%$ . In spite of the sharp discontinuities, the system still meets all of the design specifications and remains stable over the entire range of  $\pm 20\%$  error in the plant model.

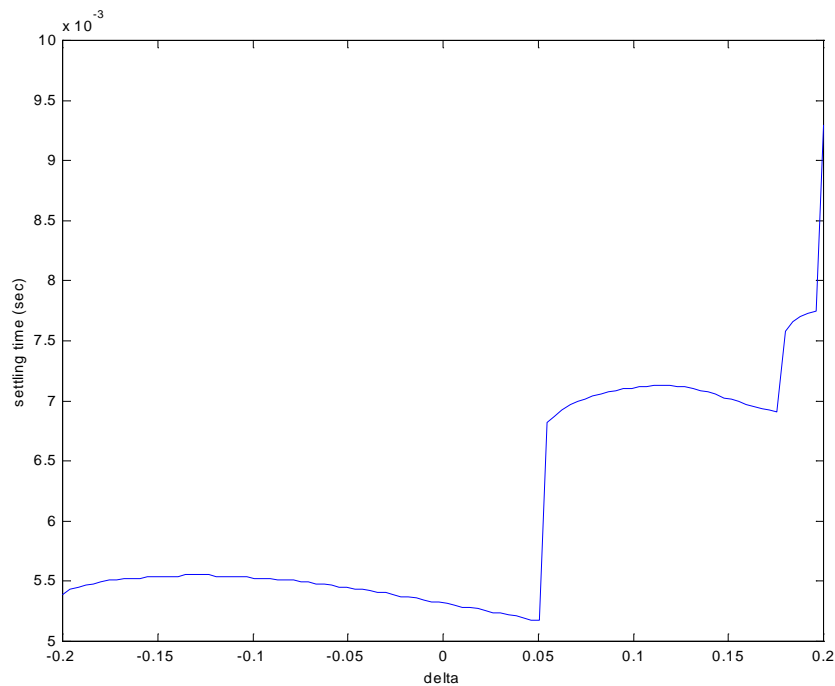


Figure 10.) Robustness analysis closed-loop compensator design

## **Conclusions**

Through this project, the design of a suitable full-state feedback compensator and an observer-based compensator has been investigated for a truncated cone with rigid end conditions. Using standard full-state feedback techniques, the following pole locations were converged upon for suitable performance given the design specifications:  $-650 \pm 863i$ ,  $-684 \pm 1509i$ , and  $-440 \pm 2425i$ . Using these pole locations as a base point, an observer-based compensator was designed using observer poles five times faster than the full-state feedback poles. Frequency response analysis of this system demonstrates stable operation of the open-loop system, while a robustness analysis illustrates acceptable operation in the presence of model errors of  $\pm 20\%$ . The overall analysis presented in this report shows that the system is in fact controllable, with a suitable compensator design that satisfies all of the design specifications set forth for the system response.

## **UPCOMING TASKS**

We plan to perform benchtop experiments to verify the analytical modal developed in this work.